TECHNISCHE UNIVERSITÄT CHEMNITZ

Sonderforschungsbereich 393

Parallele Numerische Simulation für Physik und Kontinuumsmechanik

P. Ciarlet, Jr B. Jung S. Kaddouri S. Labrunie J. Zou

The Fourier Singular Complement Method for the Poisson Problem. Part III: Implementation Issues

Preprint SFB393/05-12

Abstract

This paper is the last part of a three-fold article aimed at some efficient numerical methods for solving the Poisson problem in three-dimensional prismatic and axisymmetric domains. In the first and second parts [7][8], the Fourier singular complement method (FSCM) was introduced and analysed for prismatic and axisymmetric domains with reentrant edges, as well as for the axisymmetric domains with sharp conical vertices. In this paper we shall mainly conduct numerical experiments to check and compare the accuracies and efficiencies of FSCM and some other related numerical methods for solving the Poisson problem in the aforementioned domains. In the case of prismatic domains with a reentrant edge, we shall compare the convergence rates of three numerical methods: 3D finite element method using prismatic elements, FSCM, and the 3D finite element method combined with the FSCM. For axisymmetric domains with a non-convex edge or a sharp conical vertex we investigate the convergence rates of the Fourier finite element method (FFEM) and the FSCM, where the FFEM will be implemented on both quasi-uniform meshes and locally graded meshes. The complexities of the considered algorithms are also analysed.

Preprintreihe des Chemnitzer SFB 393

ISSN 1619-7178 (Print) ISSN 1619-7186 (Internet)

SFB393/05-12 October 2005

Contents

Author's addresses:

Patrick Ciarlet[1]
Samir Kaddouri
ENSTA-CNRS-INRIA UMR 2706
32, boulevard Victor
75739 Paris Cedex 15 (France)

Beate Jung[2]
Fakultät für Mathematik
Technische Universität Chemnitz
D-09107 Chemnitz (Germany)

Simon Labrunie
IECN
Université Henri Poincaré Nancy I & INRIA (Projet CALVI)
54506 Vandœuvre-lès-Nancy cedex (France)

Jun Zou[3]
Department of Mathematics
The Chinese University of Hong Kong
Shatin, N.T. (Hong Kong)

[1]This author was supported in part by France/Hong Kong Joint Research Scheme
[2]This author was supported by DGA/DSP-ENSTA 00.60.075.00.470.75.01 Research Programme
[3]This author was fully supported by Hong Kong RGC grants (Project 403403 and Project CUHK4048/02P)

1 Introduction

Numerical solutions of three-dimensional boundary value problems (BVPs) in non-convex domains are quite different from the two-dimensional case and is usually much more difficult. Among many existing methods, Fourier Finite Element Method (FFEM) is a popular and widely investigated efficient method for solving BVPs in three-dimensional prismatic or axisymmetric domains. The method uses the Fourier expansion in one space direction and the finite element method in the other two space dimensions, see, for example, [5, 12, 13, 16, 19]. It is known that when reentrant edges are present in the domains (or sharp conical vertices characterized by [8, Eq. (3)] in axisymmetric domains), FFEM can not achieve the optimal H^1-convergence rate due to the singularities of the solution. In order to overcome this disadvantage, the Fourier Singular Complement Method (FSCM) has been developed in [7, 8] for solving the singular Poisson problem. One special feature of this new method is to add some singular test functions to the usual Lagrange FEM, but in a completely different manner from the existing ones. The FSCM has the following advantages: no any cut-off functions are required in its computation; singularity coefficients need to be evaluated only for low Fourier modes; and no any mesh grading or refinements are needed to achieve the optimal convergence near the singular edges or vertices so that the application to unsteady problems with larger time steps is possible.

The aim of this paper is to test the efficiency of the FSCM, and to compare it with the efficiency of some other popular numerical methods for solving the Poisson problem with homogeneous boundary conditions. In the case with non-homogeneous boundary conditions, one may consider a suitable lifting to transform the original problem into a homogenous one. In the case of a prismatic domain we will test three numerical methods: 3D finite element method using prismatic elements, the FSCM, and the 3D FEM combined with the FSCM. The latter is motivated by the fact that the edge singularity distribution is in general not explicitly known, but it can be approximated by means of a Fourier series of the 2D singularity coefficients which can be computed by the FSCM. Then the regular part of the solution can be approximated by the usual 3D FEM to the Poisson problem with a modified right-hand side. For axisymmetric domains we shall also conduct numerical experiments for three different methods: the FSCM, the FFEM on quasi-uniform meshes as well as on meshes with appropriate local grading. We remark that the algorithm of the FSCM for the BVP in axisymmetric domains may differ slightly, depending on whether reentrant edges or sharp conical vertices are present. There are three pairs of dual/primal singular functions for reentrant edges, but only one pair for conical vertices [8].

The rest of this paper is arranged as follows. In Section 2, the convergence rates of different numerical methods are tested for solving the Poisson problem in prismatic domains, and the influence of the regularity of the right-hand side on the convergence rate of the FSCM is also investigated. Section 3 presents numerical results for axisymmetric domains. Due to the presence of the weighting factor r^{-1}, where r is the distance to the symmetry axis, in the considered bilinear forms, we shall test two problems whose exact solutions behave differently near the symmetry axis. Furthermore, we investigate whether the convergence rate, as a function of the number N of Fourier modes used, depends on the regularity of the exact solution (consequently on the regularity of the right-hand side) with respect to the rotational angle. Finally, some complexity analysis is given in Section 4

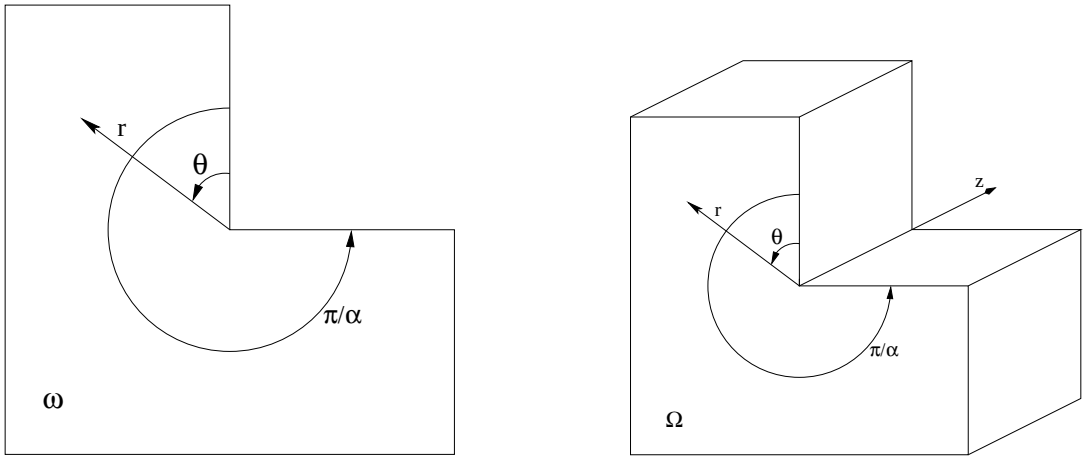

Figure 1: 2D and 3D domains.

for the numerical methods considered.

2 Numerical results for prismatic domains

We are interested in the numerical solution of the following homogeneous Dirichlet problem for the Poisson equation

$$-\Delta u \;=\; f \quad \text{in} \quad \Omega\,; \quad u = 0 \quad \text{on} \;\; \partial\Omega \tag{1}$$

in prismatic domains with reentrant edges. Typically, the domain Ω is described by $\omega \times Z$ with ω being a polygonal domain having a reentrant corner of angle $\dfrac{\pi}{\alpha}, \alpha \in]\dfrac{1}{2}, 1[$ and Z an interval. The numerical tests to be presented in this section are made over the prismatic domain of Figure 1, where

$$\omega =]2,4[\times]1,3[\setminus]3,4[\times]2,3[,\;\; \alpha = \frac{2}{3} \;\text{and}\;\; Z =]0,1[,$$

so domain Ω possesses only one reentrant edge $E = C\times]0,1[$, with C being the reentrant corner of ω. We remark that we take a polygon ω with only one reentrant edge here is purely for the sake of simplicity.

It is well known from [10, 11] that the solution u to the Poisson system (1) has, in general, a singular behaviour near the non-convex edge and corners. Precisely, it is shown in [1, 20] that in the prismatic case, corner singularities behave as the edge singularity, and the solution u can be split into

$$u = u_r + \gamma(r,z) r^{\alpha} \sin(\alpha\theta), \tag{2}$$

where u_r is the regular part, i.e. $u_r \in H^2(\Omega)$, $\gamma(r,z)$ is the edge singularity distribution and (r,θ,z) are the local cylindrical coordinates.

The poor regularity of u, $u \in H^s(\Omega)$ for any $s < 1 + \alpha$, makes the piecewise linear Lagrange finite element method (FEM) converge in H^1-norm only at the rate h^α. So the Singular Complement Method [9] was combined in [7] with the Fourier expansion along the singular edge to recover an optimal convergence order $\mathcal{O}(h + N^{-1})$ with the piecewise linear Lagrange FEM, when the right-hand side f meets certain regularity conditions: $f \in H^2(]0,1[, L^2(\omega)) \cap H_0^1(]0,1[, L^2(\omega))$. Here h is the finite element mesh size and N is the number of Fourier modes used. These conditions will be examined through numerical experiments below. Three numerical methods will be used to solve the 3D Poisson problem (1) and their convergence rates will be compared. The first method is the finite element method using 3D prismatic elements (without any refinement), and it is motivated by the prismatic shape of domain Ω. The theoretical convergence rate of this method is h^α. The second method is the FSCM proposed in [7], while the third method uses the SCM to approximate the singular part and then use it to discretize the regular part by prismatic finite elements. We remark that in this last method, Inverse Fourier Transform is needed only for reconstructing the singular part. All numerical tests are carried out with MATLAB. Some complexity analysis will be presented in Section 4 for these numerical methods.

2.1 Approximation of the solution using prismatic finite elements

In this section, we will test the convergence rate of the finite element method using 3D prismatic elements for solving the Poisson problem (1). For the purpose, we triangulate $\bar{\Omega}$ into small equal prisms of mesh size h with vertices $\{M_i\}_{i=1}^N$, and the resulting triangulation is denoted by $\mathcal{P}_h$. Clearly, one may realize $\mathcal{P}_h$ by a 2D regular triangulation of $\bar{\omega}$ and a 1D partition of the interval Z, both with mesh size h. On $\mathcal{P}_h$, we define the following

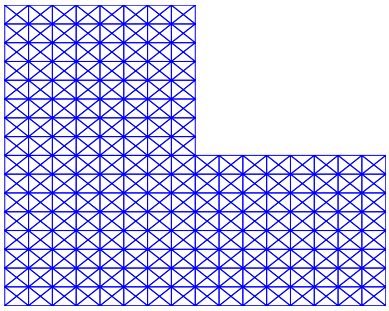

Figure 2: Two dimensional mesh for $h = 0.125$.

prismatic finite element space :

$$V_h = \{v_h \in \mathcal{C}^0(\bar{\Omega}) : \ v_h|_Q \in P_{2D}^1 \otimes P_{1D}^1, \ \forall Q \in \mathcal{P}_h\}$$

and its subspace V_h^0 with functions vanishing on the boundary of Ω. Each shape function ϕ_j of V_h satisfies $\phi_j(M_i) = \delta_{i,j}$ and reads on each element as follows (cf. [6]):

$$\phi_j(x, y, z) = a_1yz + a_2xz + a_3z + a_4x + a_5y + a_6.$$

Then the Poisson problem (1) can be naturally approximated by the discrete problem:

Find $u_h \in V_h^0$ such that

$$\int_\Omega \nabla u_h \cdot \nabla v_h d\Omega = \int_\Omega f v_h d\Omega \quad \forall\, v_h \in V_h^0.$$

h	Prisms	Nodes	$\|u - u_h\|_1$	β_1
0.25	768	565	4.10e-3	-
0.125	6144	3753	2.38e-3	0.78
0.0625	49152	27217	1.33e-3	0.84
0.03125	393216	207009	7.44e-4	0.84

Table 1: H^1-norm errors.

The errors are computed with a 14 point quadrature formula in each prism, obtained from a 2D 7 point formula (5^{th}-order) and 1D 2 point formula (3^{rd}-order). Table 1 presents the H^1-norm errors of the prismatic finite element solution described above when the exact solution is constructed as follows :

$$u(r, \theta, z) = \begin{cases} (z(1-z))^2 \left(1 - (2r)^{\frac{4}{3}} + (2r)^{\frac{5}{3}} - (2r)^2\right)^2 r^{\frac{2}{3}} \sin(\frac{2}{3}\theta) & , \quad r \leq \frac{1}{2}, \\ 0 & , \quad r \geq \frac{1}{2} \end{cases}$$

The values β_1 in Table 1 represent the convergence rates in the form $O(h^{\beta_1})$ and are computed using the H^1-norm errors on two consecutive meshes. We see from Table 1 that the H^1 convergence rate is slightly better than the theoretical one $O(h^{\frac{2}{3}})$ but still worse than $O(h)$. The difference between the exact and the observed rates may be due to the use of quasi uniform meshes and the presence of a truncation function.

The next section will be dedicated to show the remarkable accuracy of the FSCM proposed in [7] for prismatic domains. The theoretical convergence is proved to be optimal when $f \in H^2(]0, 1[, L^2(\omega))$ and satisfies the homogeneous boundary conditions at the faces $z = 0$ and $z = 1$. This motivates another interesting investigation into the effect of the boundary conditions of f at the faces $z = 0$ and $z = 1$ on the convergence rate of the method (see [7, Theorem 6.1]), as well as how this convergence rate depends on the regularity of f with respect to z.

2.2 Convergence of the Fourier Singular Complement Method (FSCM)

The FSCM is based on a Fourier expansion along the edge direction (z-axis) to transform the 3D problem into a sequence of 2D problems which are then solved using the 2D SCM.

One of the nice features of the FSCM is that it needs to compute the singularity coefficients in the 2D problems only for low Fourier modes, whereas for higher modes the singular part is sufficiently small so that the discretization error dorminates. Before stating the algorithm we introduce a few notations. N is the number of Fourier modes used and $C^\star$ is a positive constant. We denote by a_k the bilinear form on $H_0^1(\omega) \times H_0^1(\omega)$ defined by

$$a_k(u,v) = \int_\omega (\nabla u \cdot \nabla v + k^2\pi^2 uv) d\omega.$$

Let $\mathcal{T}_h$ be a regular triangulation of $\overline{\omega}$, we then define

$$W_h^0 = \left\{ u \in \mathcal{C}(\overline{\omega}), u_{|K} \in P^1(K)\ \forall K \in \mathcal{T}_h \right\} \cap H_0^1(\omega)$$

to be the 2D P^1 Lagrange finite element space. The FSCM algorithm can be stated as follows: For $k \leq N$,

1. Find $z_h^k \in W_h^0$ such that $a_k(z_h^k, v_h) = (f^k, v_h)\ \forall v_h \in W_h^0$,

2. Set $c_h^k = \begin{cases} \frac{(f^k - (k\pi^2)^2 z_h^k, p_s^h)}{\|p_s^h\|^2}, & \text{if } k < C^\star h^{-\frac{1}{2-\alpha}} \\ 0\,, & \text{otherwise} \end{cases}$

3. Find $\tilde{u}_h^k \in W_h^0$ such that $a_k(\tilde{u}_h^k, v_h) + c_h^k a_k(\phi_s^h, v_h) = (f^k, v_h)\ \ \forall v_h \in W_h^0$,

where p_s^h, ϕ_s^h are respectively the approximate dual and primal singular function, the exact ones having the expressions:

$$\begin{aligned} p_s &= \tilde{p} + r^{-\alpha}\sin(\alpha\theta), \qquad \tilde{p} \in H^1(\omega), \\ \phi_s &= \tilde{\phi} + \beta r^\alpha \sin(\alpha\theta), \qquad \tilde{\phi} \in H^2(\omega),\ \beta = \frac{1}{\pi}\|p_s\|_0^2, \end{aligned}$$

cf.[7, §5] for more details. Then the approximate solution to the Poisson problem (1) is given by

$$u_h^N = \sum_{k=0}^{k=N} u_h^k(x,y)\sin(k\pi z), \quad u_h^k = \tilde{u}_h^k + c_h^k \phi_s^h. \tag{3}$$

Unlike in the axisymmetric case where no boundary conditions regarding θ are needed thanks to the periodicity, one has to assume in the prismatic case that f vanishes at $z = 0$ and $z = 1$ in order to derive the optimal convergence of order $O(N^{-1} + h)$ (cf. [7, Theorem 6.1]. To test the actual effect of the boundary conditions of f on the accuracy of the FSCM solution, we use a right hand side f which does not satisfy the vanishing boundary conditions on $\partial\omega \times \{0,1\}$ but has the required regularity in z (cf. [7]), namely $f \in H^2(]0,1[, L^2(\omega))$. We suppose the exact solution is

$$u(r,\theta,z) = \begin{cases} z(1-z)\left(1 - (2r)^{\frac{4}{3}} + (2r)^{\frac{5}{3}} - (2r)^2\right)^2 r^{\frac{2}{3}}\sin(\frac{2}{3}\theta), & r \leq \frac{1}{2}, \\ 0, & r \geq \frac{1}{2} \end{cases} \tag{4}$$

for which the edge singularity coefficient is constructed in $H^2(]0,1[) \cap H_0^1(]0,1[)$. In our computations, the FSCM solution u_h^N in (3) is computed with N Fourier modes and u_h^k is computed on the triangulation $\mathcal{T}_h$ of ω with mesh size h. To study the convergence rate in terms of h, we take the number of Fourier modes to be the same for all meshes and to satisfy $N^{-1} \leq h$ for the finest mesh. The convergence of the FSCM solution is reported in

h	Nodes	$k_{\max}$	$\|u - u_h\|_1$	β_1
0.125	417	4	8.04e-3	-
0.0625	1601	7	4.32e-3	0.90
0.0312	6273	13	2.15e-3	0.99

Table 2: H^1-norm errors by the FSCM using $N = 32$ Fourier modes.

Table 2, where $k_{\max}$ is the highest mode used in the SCM whose dependence on the mesh size h is given in Figure 3, and the constant $C^\star$ is set to the value one. We see from Table

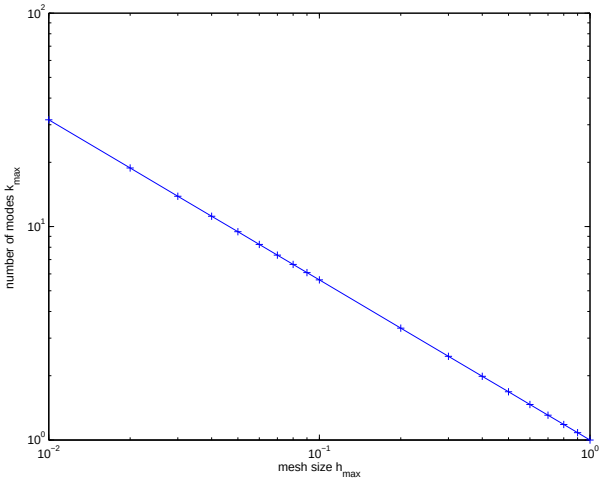

Figure 3: Graph of $k_{\max} = [h^{-\frac{1}{2-\alpha}}]$ where $[x]$ denotes the integer part of x with $\alpha = \frac{2}{3}$.

2 that the H^1 rate of convergence of FSCM is optimal even if f does not vanish at $z = 0$ and $z = 1$. This leads us to investigate the effect of the regularity of the right-hand side with respect to z. Thanks to the spectrum of the one dimensional operator:

$$-\frac{d^2}{dz^2} : H_0^1(]0,1[) \to H^{-1}(]0,1[),$$

we know by interpolation that

$$[H_0^1(]0,1[), L^2(]0,1[)]_s = \left\{ f = \sum_{k=1}^{\infty} f^k \sin(k\pi z) : \sum_{k=0}^{\infty} (k\pi)^{2(1-s)} |f^k|^2 < \infty \right\}$$

is $H_0^{1-s}(]0,1[)$ for $s \neq \frac{1}{2}$ and $H_{00}^{\frac{1}{2}}(]0,1[)$ for $s = \frac{1}{2}$ (cf. [15]). In Table 3, optimal numerical convergence rates are observed for f with different regularities, lying respectively in the

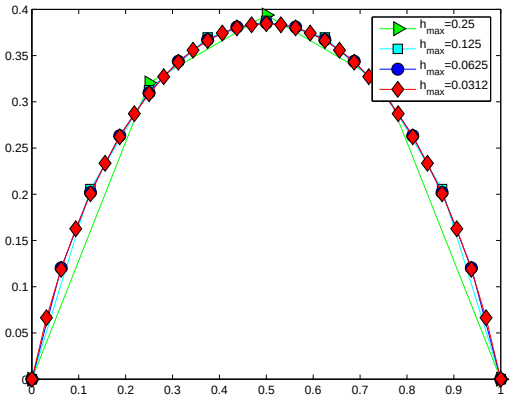

Figure 4: Edge singularity distribution γ_h for different mesh sizes h with $f = 1$.

spaces $H_0^{1-s}(]0,1[;L^2(\omega))$ for $s = 0, \frac{1}{4}, \frac{3}{4}, 1$ and $H_{00}^{\frac{1}{2}}(]0,1[;L^2(\omega))$ for $s = \frac{1}{2}$. These tests were done without FFT but with the real Fourier modes of the right-hand side. Indeed, considering FFT or not does not bring any obvious difference in our results. The exact Fourier modes of the solution are

$$u_k(r,\theta) = \begin{cases} \dfrac{1}{(k\pi)^{\frac{7}{2}-s+\varepsilon}} \left(1-(2r)^{\frac{4}{3}}+(2r)^{\frac{5}{3}}-(2r)^2\right)^2 r^{\frac{2}{3}} \sin(\dfrac{2}{3}\theta), & r \le \frac{1}{2}, \\ 0, & r \ge \frac{1}{2} \end{cases}$$

They are chosen to ensure the condition

$$(k\pi)^{2(1-s)} \|f^k\|_0^2 \sim \frac{1}{(k\pi)^{1+2\varepsilon}},$$

for a small $\varepsilon > 0$.

s	0	$\frac{1}{4}$	$\frac{1}{2}$	$\frac{3}{4}$	1
β_1	0.97	1.00	1.03	1.03	1.02

Table 3: H^1-norm convergence rate for f in $H_0^{1-s}(]0,1[;L^2(\omega))$, $s \neq \frac{1}{2}$ and $H_{00}^{\frac{1}{2}}(]0,1[,L^2(\omega))$, $N = 32$.

Thanks to [7, Ineq. (25)], see also [3], the edge singularity distribution γ belongs to $H^{1-\alpha}(]0,1[)$, but when f has a $\mathcal{C}^\infty$ regularity in $\bar{\Omega}$, γ is in $\mathcal{C}^\infty([0,1])$, as it is proved in [10]. Figure 4 represents the approximate singularity distribution γ_h for $f = 1$ with different mesh sizes : the fact that γ_h vanishes at the end points of the edge is an artifact due to the truncation of the Fourier series. Nevertheless, $\{\gamma_h\}_h$ seems to converge to a regular limit that vanishes at $z = 0$ and $z = 1$. It is also interesting to see what happens to the case where f is not smooth : Figure 5 shows the edge singularity distribution for the data $f(z) = \log(|\log(\frac{z}{2})|)$ which is in $H^{\frac{1}{2}}(]0,1[)$. Interestingly, the family $\{\gamma_h\}_h$ seems to converge, but only outside a neighborhood of $z = 0$.

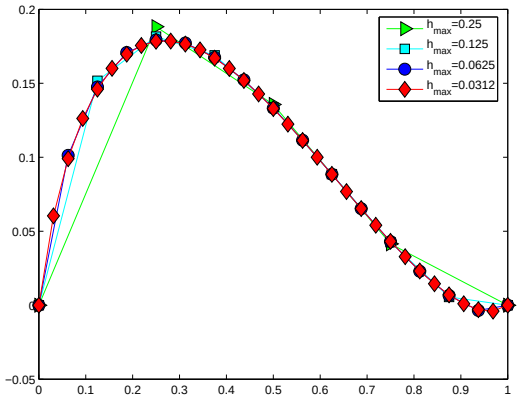

Figure 5: Representation of the edge singularity distribution for $f(z) = \log(|\log(\frac{z}{2})|)$ for different mesh sizes h.

2.3 Combination of the 3D FEM with the FSCM

The FSCM reduces the three dimensional Poisson problem (1) to a sequence of 2D problems. In this section, we are interested in a new method that combines the 3D FEM with the FSCM. The basic idea is to make use of the singular part of the exact solution to compute its regular part by means of the 3D prismatic finite elements. As the edge singularity distribution $\gamma(r, z)$ in (2) is not known explicitly for general right-hand side $f \in L^2(\Omega)$, we assume as in [7] some additional regularity on f, namely $f \in H^2(]0,1[, L^2(\omega)) \cap H_0^1(]0,1[, L^2(\omega))$. Then one can write the singular part simply as $\gamma(z)\phi_s$ with $\gamma \in H^2(]0,1[) \cap H_0^1(]0,1[)$. Letting

$$\gamma_h(z) = \sum_{k=0}^{N(h)} c_h^k \sin(k\pi z), \quad N(h) = k_{\max} = [h^{-\frac{1}{2-\alpha}}], \tag{5}$$

be the approximate singularity distribution obtained by the FSCM, we can then compute the regular part of the solution using the prismatic finite elements as described in Section 2.1. In fact, by writing the solution as

$$u = u_r + \gamma\phi_s,$$

with $\gamma \in H^2(]0,1[) \cap H_0^1(]0,1[)$, we know that the regular part u_r solves the following boundary value problem:

$$-\Delta u_r = f + (\gamma''\phi_s - \gamma p_s) \ \text{ in } \Omega\,; \quad u_r = 0 \ \text{ on } \partial\Omega,$$

where p_s, ϕ_s are defined as in FSCM. Since u_r and γ are both H^2-regular, the prismatic finite element approximation of u_r has an optimal convergence while the approximation of γ by γ_h in (5) has a first order accuracy, cf. [7, Ineq. (68)]. The convergence of this combined 3D FEM with the FSCM is shown in Table 4 when f is associated with the exact solution (4) of the previous section. Once again, we see that the optimal rate of

h	3D Nodes	2D Nodes	$\|u-u_h\|_1$	β_1
0.25	565	113	1.24e-2	-
0.125	3753	417	7.80e-3	0.65
0.0625	27217	1601	4.22e-3	0.88
0.0312	207009	6273	2.13e-3	0.98

Table 4: H^1-norm errors by using the FSCM for the singular part and prismatic finite elements for the regular one.

convergence for the H^1 error is recovered. Noting $\gamma \in H^2(]0,1[) \cap H_0^1(]0,1[)$, so its Fourier approximations γ_h converge in $H^2(]0,1[) \cap H_0^1(]0,1[)$ (cf. [7, Lemma 6.1]; in this case the conclusion holds without assuming the boundary conditions on f), therefore the optimal convergence rate can be recovered in this example. Also, one can observe that the errors are almost identical to the ones as shown in Tables 2.

To summarize, one can conclude that the FSCM is indeed powerful and robust, since it yields satisfactory results even though the vanishing boundary condition on f is not satisfied (at least when the edge singular function lies in some suitable space). We will analyse in Section 4 the complexity of these methods, which shall indicate that the FSCM is less expensive.

3 Numerical results for axisymmetric domains

The aim of this section is to compare two different methods for solving the BVP (1) in axisymmetric domains with reentrant edges or sharp conical vertices. The first method is the FSCM [8], while the second is called the FFEM, which is a combination of the Fourier method with the FEM in 2D (cf. [12, 16]). The convergence rates of two methods in terms of the mesh size h and the number N of the Fourier modes used will be investigated. It is known (e.g. [13]) that the FFEM on quasi-uniform meshes can not achieve *optimal* convergence in terms of h, due to the singularity of the solution. So we shall test the convergence of FFEM on some locally graded meshes and compare it with the FSCM (cf. [8]). The numerical experiments are carried out by means of the package FEMGP, that is described in [14]. More details can be found in Section 4 about the numerical realization of the considered algorithms.

Let (r, θ, z) be the natural cylindrical coordinates. We suppose that the axisymmetric domain Ω is generated by rotation of a polygon ω, called the meridian domain, about the z-axis. Furthermore, γ_b denotes that part of $\partial\omega$ which generates the boundary of the 3D domain Ω (see [8, §2] for more details concerning geometric setting and notations).

Applying the Fourier analysis with respect to θ to the functions u and f in (1), with a Fourier expansion like $u = \sum_k u^k e^{\imath k\theta}$, we know that for any k, the Fourier mode u^k is

characterized as the solution to the following 2D boundary value problem :

$$-\frac{\partial^2 u^k}{\partial r^2} - \frac{1}{r}\frac{\partial u^k}{\partial r} - \frac{\partial^2 u^k}{\partial z^2} + \frac{k^2}{r^2}\, u^k \;=\; f^k \qquad \text{in } \omega\,; \quad u^k = 0 \quad \text{on } \gamma_b\,. \tag{6}$$

The variational formulation of (6) reads as follows (cf. [8, §2.3]) :

$$a_k(u^k, v) = (f^k \mid v) \quad \forall v \in V_{(k)},$$

where $V_{(k)}$ is a Sobolev space described in [8, Lemma 2.1], and

$$a_k(u, v) := \iint_\omega \Big[r\, \nabla u \cdot \nabla \overline{v} + \frac{k^2}{r}\, u\, \overline{v} \Big] dr dz, \quad (f \mid v) := \iint_\omega f\, \overline{v}\, r dr dz, \tag{7}$$

with ∇ being the gradient in the (r, z) plane.

3.1 The FFEM and the FSCM for domains with reentrant edges

We will consider in this subsection the axisymmetric domain whose meridian domain possesses a single reentrant corner on γ_b, and the domains with sharp conical vertices will be studied in Subsection 3.2.

In order to describe the FFEM on locally graded meshes, we first introduce some notations. We use (r_E, z_E) to denote the coordinates of the singular corner E of ω, and (ρ, ϕ) to denote the local polar coordinates with respect to E:

$$r - r_E = \rho\, \cos(\phi + \phi_0), \quad z - z_E = \rho\, \sin(\phi + \phi_0). \tag{8}$$

To provide a framework for graded meshes, we introduce the real grading parameter μ $(0 < \mu \le 1)$, the grading function ρ_j, the step size h_j and regions of mesh grading B_j as follows:

$$\begin{aligned} \rho_j &:= \tilde{\rho}\,(jh)^{\frac{1}{\mu}}, && j = 0, 1, \ldots, J \\ h_j &:= \rho_j - \rho_{j-1}, && j = 1, 2, \ldots, J \\ B_j &:= \{(r, z) \in \omega : \rho_{j-1} < \rho \le \rho_j\}, && j = 1, 2, \ldots, J, \end{aligned}$$

with $J = [h^{-1}]$ (integer part of h^{-1}) and some real parameter $\tilde{\rho}$, $0 < \tilde{\rho} < r_E$. The coordinates ρ, ϕ are related with r and z by (8). We suppose that the triangulation $\mathcal{T}_h$ of the domain ω fulfills the following assumptions (cf. [17, 1]):

(i) $l_1 h \le h_T \le l_2 h$ for $T \in \mathcal{T}_h$: $T \cap B_j = \emptyset$ for $j = 1, \ldots, J$,

(ii) $l_1 h_j \le h_T \le l_2 h_j$ for $T \in \mathcal{T}_h$: $T \cap B_j \neq \emptyset$ at least for one $j \in \{1, \ldots, J\}$,

where l_1, l_2 do not depend on h. Let n_j denote the number of triangles satisfying $T \cap B_j \neq \emptyset$ for any $j \in \{1, \ldots, J\}$, then by elementary considerations it holds that $n_j \le Cj$ for $j = 1, \ldots, J$, with C independent of h and j. Clearly, for $\mu = 1$ the mesh is quasi-uniform,

for $0 < \mu < 1$ it is quasi-uniform only outside the region of grading the mesh. But the total number of nodes of $\mathcal{T}_h$ is always of the order $\mathcal{O}(h^{-2})$. Related types of mesh grading are described e.g. in [4, 18]. The package FEMGP contains a generator for meshes satisfying the assumptions mentioned above. Some examples of meshes with such gradings are given in Figures 8.1 and 8.2.

Next, we shall recall the FSCM algorithm for the axisymmetric case [8, §§5.3 and 5.5], which is slightly different from that in the prismatic case. The algorithm reads as follows:

1. Find $z_h^k \in W_h^0$ such that $a_k(z_h^k, v_h) = (f^k \mid v_h)\ \forall v_h \in W_h^0$.
2. Compute $c_h^k = \begin{cases} \frac{1}{\|p_s^h\|_{0,1}^2}\Big[\big(f^k \mid p_s^h\big) - (k^2-4)\,\big(z_h^k \mid q_s^h\big)\Big], & \text{if } k < C^* h^{-\frac{1}{2-\alpha_0}} \\ 0\,, & \text{otherwise.} \end{cases}$
3. Find $\tilde{u}_h^k \in W_h^0$ such that $a_k(\tilde{u}_h^k, v_h) + c_h^k\, a_k(\varphi_s^h, v_h) = (f^k \mid v_h)\ \forall v_h \in W_h^0$,

where $\alpha_0 \in]\frac{1}{2}, \alpha[$ with α being the exponent of singularity, p_s^h and φ_s^h are respectively the approximate dual and primal singular function, and $q_s^h := p_s^h / r^2$. The bilinear form a_k and the scalar product $(\cdot \mid \cdot)$ are taken from (7), $\|\cdot\|_{0,1}$ denotes the norm associated with this scalar product. The FSCM solution is then obtained from

$$u_h^N = \sum_{k=-N}^{k=N} u_h^k(r,z) e^{ik\theta}\,, \quad u_h^k = \tilde{u}_h^k + c_h^k\, \varphi_s^h.$$

We would like to point out that the FSCM algorithm for the Poisson problem in axisymmetric domains with reentrant edges requires the computation of three pairs of dual/primal singular functions (in constrast to the prismatic case where only one pair is needed), namely $p_s^{0,e;h}$ and $\varphi_s^{0,e;h}$, $p_s^{1;h}$ and $\varphi_s^{1;h}$ as well as $p_s^{2;h}$ and $\varphi_s^{2;h}$ [8, §5].
The exact dual singular functions are (with the notation from (8) and $a := r_E$):

$$\begin{aligned}
p_s^{0,e} &= \widehat{p}^{\,0,e} + p_p^{0,e} \ \text{ with } \widehat{p}^{\,0,e} \in H_1^1(\omega), \ \ p_p^{0,e} = \rho^{-\alpha}\sin(\alpha\phi)\Big[1 - \frac{\rho}{2a}\cos(\phi+\phi_0)\Big], \\
p_s^{1} &= \widehat{p}^{\,1} + p_p^{1} \quad \text{ with } \widehat{p}^{\,1} \in V_1^1(\omega), \quad p_p^{1} = \rho^{-\alpha}\sin(\alpha\phi)\,\frac{r}{a}\Big[1 - \frac{3\rho}{2a}\cos(\phi+\phi_0)\Big], \qquad (9) \\
p_s^{2} &= \widehat{p}^{\,2} + p_p^{2} \quad \text{ with } \widehat{p}^{\,2} \in V_1^1(\omega), \quad p_p^{2} = \rho^{-\alpha}\sin(\alpha\phi)\left(\frac{r}{a}\right)^2\Big[1 - \frac{5\rho}{2a}\cos(\phi+\phi_0)\Big],
\end{aligned}$$

and the exact primal singular functions:

$$\begin{aligned}
\varphi_s^{0,e} &= \tilde{\varphi}^{0,e} + \delta^{0,e}\varphi_P^{0,e} \ \text{ with } \tilde{\varphi}^{0,e} \in V_1^1(\omega), \quad \varphi_P^{0,e} = \rho^{\alpha}\sin(\alpha\phi), \\
\varphi_s^{1} &= \tilde{\varphi}^{1} + \delta^{1}\varphi_P^{1} \quad \text{ with } \tilde{\varphi}^{1} \in V_1^2(\omega), \quad \varphi_P^{1} = \rho^{\alpha}\sin(\alpha\phi)\,\frac{r}{a}, \qquad (10) \\
\varphi_s^{2} &= \tilde{\varphi}^{2} + \delta^{2}\varphi_P^{2} \quad \text{ with } \tilde{\varphi}^{2} \in V_1^2(\omega), \quad \varphi_P^{2} = \rho^{\alpha}\sin(\alpha\phi)\left(\frac{r}{a}\right)^2.
\end{aligned}$$

The spaces $H_1^m(\omega)$ consist of all functions $w \in L_\alpha^2(\omega)$ such that their partial derivatives of order $\le m$ belong to $L_\alpha^2(\omega)$, where $L_\alpha^2(\omega)$ is defined as the set of measurable functions w

with $\|w\|_{L^2_\alpha(\omega)} = \left(\int\limits_\omega w^2(r,z) r^\alpha dr dz\right)^{\frac{1}{2}} < \infty$. The spaces $V_1^m(\omega)$ are characterized as follows: $V_1^m(\omega) = \left\{w \in H_1^m(\omega);\ \partial_r^l w|_{\partial\omega\setminus\gamma_b} = 0,\ 0 \le l < m-1, \text{ and } \partial_r^{m-1} w \in L^2_{-1}(\omega)\right\}$. The coefficients $\delta^{0,e}$ and δ^k $(k = 1, 2)$ in (10) are defined by: $\delta^{0,e} = \frac{1}{a\pi}\|p_s^{0,e}\|^2_{0,1}$, $\delta^k = \frac{1}{a\pi}\|p_s^k\|^2_{0,1}$ $(k = 1, 2)$, where $\|\cdot\|_{0,1}$ means the norm associated with the scalar product $(\cdot \mid \cdot)$ from (7). The presence of various dual/primal singular functions is basically due to different regularities of the Fourier modes u^0, $u^{\pm 1}$, and u^k with $|k| \ge 2$.

To measure the convergence rate approximately, we adopt the following asymptotic relation of the error function

$$\|u - u_h^N\|_{H^1(\Omega)} \approx C_1 h^\beta + C_2 N^{-\gamma} \tag{11}$$

where u and u_h^N are respectively the exact solution of (1) and the FSCM (or FFEM) solution, while β and γ are respectively the convergence rates with respect to h and N. By using the package FEMGP, we can obtain the norms of the error $(u - u_h^N)$ with respect to h and N separately. Therefore the values of β (or γ) can be computed by using the errors on two consecutive levels of h (or N), see [19, §6.2.1] or [13, §7] for more details.

As our first example we consider the solution of (1) in an axisymmetric domain whose meridian domain is L-shaped: $\omega :=]0,1[\times]0,1[\setminus]0.5,1[\times]0.5,1[$. Consequently, the singular corner of the meridian domain is the point $E = (r_E, z_E) = (0.5, 0.5)$, the angle ϕ_0 in (8) is $\frac{\pi}{2}$, and the exponent of singularity is $\alpha = \frac{2}{3}$. We suppose that the exact solution of the Poisson problem is given by

$$\begin{aligned} u(r,\theta,z) &= \tilde{u}(\rho,\phi)\Theta(\theta) \quad \text{with} \\ \tilde{u}(\rho,\phi) &= \begin{cases} (-2^{\frac{7}{3}}\rho^3 + 7\cdot 2^{\frac{4}{3}}\rho^2 - 14\,\rho^{\frac{5}{3}} + \rho^{\frac{2}{3}})\,\sin(\frac{2}{3}\phi) & \text{for } \rho \le 0.5 \\ 0 & \text{for } \rho > 0.5 \end{cases} \\ \Theta(\theta) &= \begin{cases} \theta^2 - \pi\theta & \text{for } 0 < \theta \le \pi \\ \theta^2 - 3\pi\theta + 2\pi^2 & \text{for } \pi < \theta \le 2\pi\,, \end{cases} \end{aligned} \tag{12}$$

and $u(r,\theta,z)$ can be represented as an infinite Fourier series:

$$u(r,\theta,z) = \frac{8}{\pi}\sum_{k=0}^{\infty} \tilde{u}^{2k+1}(\rho,\phi)\,\sin((2k+1)\theta) \quad \text{with } \tilde{u}^{2k+1}(\rho,\phi) = \frac{\tilde{u}(\rho,\phi)}{(2k+1)^3}. \tag{13}$$

Considering the convenience in practical computations, we use the sin-cos-representation of the Fourier series instead of the complex form with $e^{ik\theta}$.

We have tested the FFEM and the FSCM on quasi-uniform meshes as well as the FFEM on locally graded meshes. In order to achieve the optimal rate of convergence for FFEM on a graded mesh, a grading parameter μ with $\mu < \alpha$ should be chosen. For $\alpha \le \mu < 1$ we would obtain a better convergence rate than in the case of quasi-uniform meshes but not the optimal rate [1]. For all experiments described in this subsection we use local grading with the parameters $\mu_2 = 1.02\alpha = 0.68$ and $\mu_3 = 0.8\alpha \approx 0.533$; $\mu_1 = 1$ corresponds to the quasi-uniform mesh. Figures 8.1 and 8.2 show the locally graded meshes with $\mu = \mu_3$ for the mesh parameters $h = 0.125$ and $h = 0.0625$.

In our implementations, it seems important to mention how we calculate the most singular part of φ_s^k, the integration of the functions $p_s^{0,e;h}$ and $p_s^{k;h}$ $(k = 1, 2)$ (cf. [8, §§5.2

and 5.4]). These functions have weak regularities in the neighbourhood of the reentrant corner because of the presence of the factor $\rho^{-\alpha}$ in $p_p^{0,e}$ and p_p^k $(k = 1, 2)$. But these functions are explicitly known (see (9)), and therefore the computation of the integral can be split into two parts: one over the subdomain $\omega_1 := \{(r, z) \in \omega : \rho \leq 0.25\}$ and the other over the remaining part $\omega_2 := \omega \setminus \omega_1$. Then the integral $\iint_{\omega_1} |p_p^k|^2 r dr dz$ can be computed analytically, and the remaining terms in the integral over ω_1 as well as the integral over ω_2 are computed numerically.

First we observe the convergence behaviour in terms of the discretization parameter h. Table 5 and Figure 7 show the numerical results, where e_{μ_i}, $i = 1, 2, 3$, (resp. e_{FSCM}) denotes the H^1-norm of the error with respect to h for the FFEM on meshes with the grading parameter μ_i (resp. for the FSCM), and β_{μ_i} (resp. β_{FSCM}) is the corresponding convergence rate. For these experiments, the discretization parameter N has been chosen as $N = h^{-1}$. The value of $k_{\max}$ in the table is determined by $k_{\max} := \left\lceil C^\star h^{-\frac{1}{2-\alpha_0}} \right\rceil$, and we set $c_h^k = 0$ for $k > k_{\max}$. We choose $C^\star = 1$ and $\alpha_0 = 0.51$ in the experiments, and one may see Remark 3.1 at the end of this subsection for some comments on the choice of these parameters.

h	e_{μ_1}	β_{μ_1}	e_{μ_2}	β_{μ_2}	e_{μ_3}	β_{μ_3}	e_{FSCM}	β_{FSCM}	$k_{\max}$
0.125	2.361e-1	–	2.072e-1	–	1.695e-1	–	1.701e-1	–	4
0.0625	1.485e-1	0.669	1.175e-1	0.818	7.957e-2	1.091	9.094e-2	0.903	6
0.0312	9.004e-2	0.722	6.463e-2	0.863	3.946e-2	1.012	4.696e-2	0.953	10
0.0156	5.401e-2	0.737	3.484e-2	0.891	1.994e-2	0.985	2.381e-2	0.980	16
0.0078	3.214e-2	0.749	1.849e-2	0.914	1.017e-2	0.971	1.197e-2	0.992	25

Table 5: H^1-norms of errors: e_{μ_1}, e_{μ_2}, e_{μ_3}, e_{FSCM}; and convergence rates β_{μ_1}, β_{μ_2}, β_{μ_3}, β_{FSCM} with respect to h for the FFEM on both quasi-uniform meshes ($\mu_1 = 1$) and locally graded meshes ($\mu_2 = 0.68$, $\mu_3 \approx 0.533$) and for the FSCM.

The convergence rates shown in Table 5 confirm the theoretically expected rates which are equal to $\frac{2}{3}$ for quasi-uniform meshes and 1 for meshes with appropriate grading ($\mu < \alpha$) and for the FSCM, see e.g. [8, 13, 16]. Comparing the errors e_{μ_3} and e_{FSCM}, one can see that the FFEM with the mesh grading parameter $\mu_3 = 0.8\alpha \approx 0.533$ yields a slightly better convergence than the FSCM for the considered example. Moreover, mesh grading with $\mu_2 = 1.02\alpha = 0.68$ leads to an improved convergence rate than on quasi-uniform meshes, but not the optimal rate.

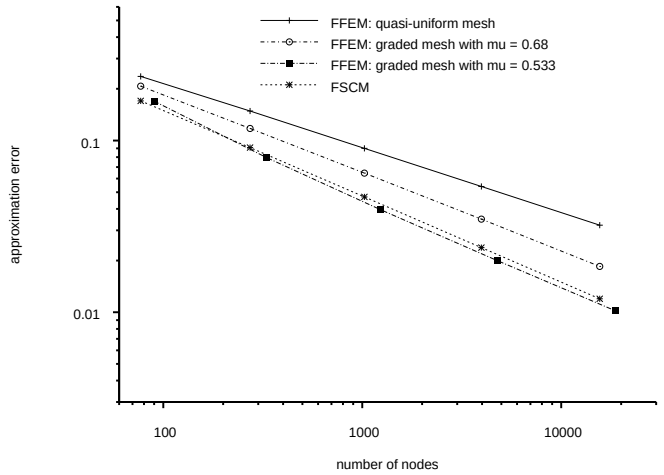

Figure 7: Representation of approximation errors for the example with the exact solution (12)

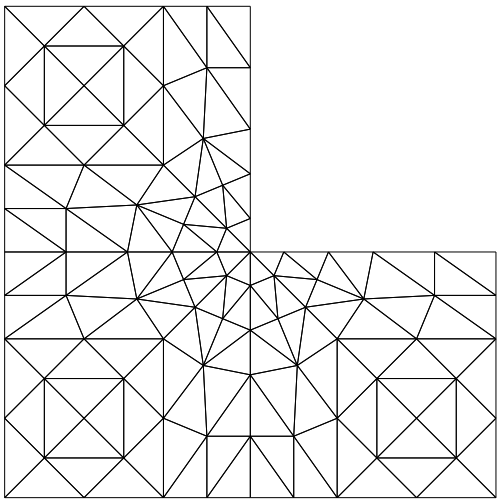

Figure 8.1: Graded mesh for $h = 0.125$ and $\mu \approx 0.533$

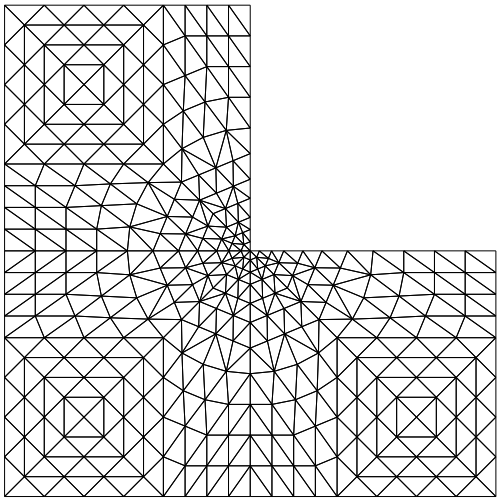

Figure 8.2: Graded mesh for $h = 0.0625$ and $\mu \approx 0.533$

The convergence behaviour of the considered methods in terms of the discretization parameter N is reported in Table 6. Same errors and convergence rates are obtained for all investigated methods, so the data are given only once in the table and the indices of e and γ are omitted. The fact that the convergences are independent of the employed methods can be justified theoretically: the singularity caused by the non-convex edge of the domain does not have any effect in direction of the rotational angle θ, and the parameters h and N are decoupled in the error estimates so mesh grading or FSCM improves only the convergence in h.

The results in Table 6 show that the convergence rate in N is considerably better than the theoretically expected rate $\gamma_{\text{th}} = 1$. This may be justified as follows: the Fourier modes of the exact solution u behaves like k^{-3} (see formula (13)), therefore the regularity of u with respect to θ is better than $H^2(]0, 2\pi[)$. But theoretically the H^2-regularity already guarantees the convergence rate $\gamma = 1$ with respect to N. So it would be interesting to

N	e	γ
8	1.3681e-3	–
16	4.5929e-4	1.5747
32	1.5985e-4	1.5227
64	5.5912e-5	1.5155
128	1.8620e-5	1.5863

Table 6: H^1-error norms e with respect to N and convergence rates γ

consider a problem whose exact solution has less regularity with respect to θ. Moreover, in view of the weighting factor r^{-1} in the bilinear forms a_k from (7), it would also be important to study an example where the Fourier modes of the solution are not equal to zero near the z-axis. This motivates our next example.

As our second example, we take the same domain Ω as in the first example, but the exact solution is represented by

$$u(r,\theta,z) = \frac{\bar{u}^0}{2} + \sum_{k=1}^{256} \frac{\bar{u}^k}{k^{\,2.51}} \sin k\theta \tag{14}$$

with $\bar{u}^k = \tilde{u}(\rho,\phi) + \hat{u}^k(r,z)$ for $k = 0,\ldots,256$, $\tilde{u}(\rho,\phi)$ from (12), and

$$\begin{aligned} \hat{u}^0(r,z) &= (12r^3 - 14r^2 + 2)\,(z^3 - 1.5z^2 + 0.5z)\,, \\ \hat{u}^k(r,z) &= (r^{3.1} - 1.5r^{2.1} + 0.5r^{1.1})\,(z^3 - 1.5z^2 + 0.5z)\,, \quad k = 1,\ldots,256. \end{aligned}$$

$\hat{u}^k(r,z)$ are added to $\tilde{u}(\rho,\phi)$ to ensure that the Fourier modes of u do not vanish in the neighbourhood of the z-axis. However, functions $\bar{u}^k(\rho,\phi)$ for $k \neq 0$ vanish right on the z-axis. This is a general property of the Fourier modes of functions $u \in H^1(\Omega)$ in axisymmetric domains Ω, see e.g. [2, 16] for more details.

h	e_{μ_1}	β_{μ_1}	e_{μ_2}	β_{μ_2}	e_{μ_3}	β_{μ_3}	e_{FSCM}	β_{FSCM}
0.125	1.708e-1	–	1.533e-1	–	1.300e-1	–	1.178e-1	–
0.0625	1.059e-1	0.690	8.631e-2	0.829	6.257e-2	1.055	6.322e-2	0.898
0.0312	6.351e-2	0.738	4.705e-2	0.875	3.122e-2	1.003	3.250e-2	0.960
0.0156	3.777e-2	0.750	2.519e-2	0.902	1.577e-2	0.985	1.642e-2	0.985
0.0078	2.234e-2	0.758	1.326e-2	0.925	8.027e-3	0.974	8.232e-3	0.996

Table 7: H^1-norms of errors: e_{μ_1}, e_{μ_2}, e_{μ_3}, e_{FSCM}; and convergence rates β_{μ_1}, β_{μ_2}, β_{μ_3}, β_{FSCM} with respect to h for the FFEM on quasi-uniform meshes ($\mu_1 = 1$), on locally graded meshes ($\mu_2 = 0.68$, $\mu_3 \approx 0.533$) and for the FSCM

Table 7 shows the convergence results with respect to h, but the values of $k_{\max}$ are not listed because they are the same as those in Table 5. We observe that the obtained

convergence rates are again very close to the ones predicted by theory. We remark that the convergence rates β_{μ_1}, β_{μ_2} are slightly better than those in Table 5. This difference can be explained as follows: the addition of the function $\hat{u}^k$ in (14) makes the regular part of $\bar{u}^k$ more dominant, therefore the convergence rates with the quasi-uniform meshes and the graded meshes with $\mu > \alpha$ are improved.

Table 8 presents the approximation errors and convergence rates with respect to N. These convergence rates agree with the theoretically predicted value $\gamma_{\text{th}} = 1$ for functions having a regularity $H^2(]0, 2\pi[)$ (but not better) with respect to θ.

N	e	γ
8	2.4070e-3	–
16	1.1731e-3	1.0370
32	5.8013e-4	1.0158
64	2.8242e-4	1.0386
128	1.2595e-4	1.1650

Table 8: H^1-norms of approximation errors with respect to N and convergence rates γ

Remark 3.1 *The choice of the parameter $C^\star$ may have some influence on the approximation errors and the convergence rates. In order to find a suitable value for this parameter, we have tried to fix $\alpha_0 = 0.51$ and compare the convergence rates obtained for $C^\star = 1$ (see Table 5) with those for $C^\star = 0.125$. In the case $C^\star = 0.125$, we have $k_{max} = 0$ for $h = 0.125$ and $h = 0.0625$, so we obtain exactly the same approximate solution as in the case of the FFEM. Consequently, the convergence rate at this level is not better than that of the FFEM. But for the smaller discretization parameters h, the convergence rates are as good as the rates presented in this subsection, although the values of k_{max} are smaller than those in Table 5. On the other hand, since the convergence rates obtained with $C^\star = 1$ are convincing, there is no use to increase the value of $C^\star$. Larger values of $C^\star$ would cause increased values of k_{max} and, consequently, an increased number of 2D problems to be solved [8, §5.3]. For fixed $C^\star = 1$, the value of k_{max} becomes larger with increasing α_0. But we have observed that their effects on the convergence rate is insignificant in all the experiments reported in this subsection. Therefore we have chosen $\alpha_0 = 0.51$, in contrast to $\alpha_0 = 2/3$ selected in Section 2.*

3.2 Numerical results for domains with sharp conical vertices

Sharp conical vertices are another type of geometric singularities occurring in an axisymmetric domain, and are defined by the condition that $\frac{\pi}{\beta} > \frac{\pi}{\beta_*} \simeq 130°48'$ (cf. [8, §2.1]). Here $\frac{\pi}{\beta}$ is the size of an interior angle of ω which belongs to a corner lying on the z-axis. The FSCM is an algorithm that is proposed in [8] to deal with such singularities. In comparison with the reentrant edge case of Subsection 3.1, only one Fourier mode, namely u^0, has a singularity. Consequently, we need an approximation for only one pair of dual/primal

singularities $p_s^{0,c}$, $\varphi_s^{0,c}$ and one singularity coefficient. The exact dual and primal singular function read as follows:

$$\begin{aligned} p_s^{0,c} &= \tilde{p}^{0,c} + p_P^{0,c} \qquad \text{with } \tilde{p}^{0,c} \in H_1^1(\omega) \text{ and } p_P^{0,c} = \rho^{-\nu_0-1} P_{\nu_0}(\cos\phi), \\ \varphi_s^{0,c} &= \tilde{\varphi}^{0,c} + \delta^{0,c}\varphi_P^{0,c} \text{ with } \tilde{\varphi}^{0,c} \in H_1^2(\omega) \text{ and } \varphi_P^{0,c} = \rho^{\nu_0} P_{\nu_0}(\cos\phi), \end{aligned} \tag{15}$$

where P_{ν_0} denotes the Legendre function with index $\nu_0 := \min\{\nu > 0 : P_\nu(\cos\frac{\pi}{\beta}) = 0\}$ [8, §2.1]. The spaces $H_1^m(\omega)$ were introduced in Subsection 3.1, and the coefficient $\delta^{0,c}$ in (15) is given by

$$\delta^{0,c} = \|p_s^{0,c}\|_{0,1}^2 \Big[(1+2\nu_0)\int_0^{\pi/\beta} P_{\nu_0}(\cos\phi)^2 \sin\phi \, d\phi\Big]^{-1},$$

with the norm $\|\cdot\|_{0,1}$ associated with the scalar product $(\cdot \mid \cdot)$ from (7).

Now, the FSCM algorithm given in Subsection 3.1 needs to be carried out only for $k = 0$, where the parameters $C^\star$, α_0 and the number $k_{\max}$ do not occur.

We now consider an axisymmetric domain whose meridian domain is a pentagon with the vertices $(0,-1)$, $(1,-1)$, $(1,1)$, $(0.41421,1)$, and $(0,0)$, see Figure 9. The corresponding axisymmetric domain has a sharp vertex with the opening angle $\frac{\pi}{\beta} = 157.5°$. Assume that the Poisson problem (1) has the exact solution of the form

$$u(r,\theta,z) = \frac{u^0(r,z)}{2} + u^1(r,z)\sin\theta \tag{16}$$

where the Fourier modes u^0 and u^1 are given by

$$\begin{aligned} u^0(r,z) &= \tilde{u}^0(\rho,\phi) = \Big(-\rho^3 + \frac{3-\nu_0}{\nu_0-1}\rho^2 + \frac{\nu_0-3}{\nu_0-1}\rho^{1+\nu_0} + \rho^{\nu_0}\Big) P_{\nu_0}^0(\cos\phi) && \text{for } \rho \le 1 \\ u^0(r,z) &= \tilde{u}^0(\rho,\phi) = 0 && \text{for } \rho > 1 \\ u^1(r,z) &= \tilde{u}^1(\rho,\phi) = (-\rho^5 + 3\rho^4 - 3\rho^3 + \rho^2)\, P_{\nu_1}^1(\cos\phi) && \text{for } \rho \le 1 \\ u^1(r,z) &= \tilde{u}^1(\rho,\phi) = 0 && \text{for } \rho > 1 \end{aligned}$$

with $P_{\nu_0}^0(\cos\phi)$ (resp. $P_{\nu_1}^1(\cos\phi)$) above being the Legendre function with indices $\nu_0 \approx 0.29225$ and 0 (resp. $\nu_1 \approx 1.06783$ and 1). It is natural for us to consider only the convergence with respect to the discretization parameter h with this example. Noting that $u^0 \in H^{\nu_0+\frac{3}{2}-\varepsilon}(\omega)$ for $\varepsilon > 0$, we choose the parameters $\mu_2 = 1.02(\nu_0 + \frac{1}{2}) \approx 0.808$ and $\mu_3 = 0.8(\nu_0 + \frac{1}{2}) \approx 0.634$ for the local mesh grading near the singular point $(0,0)$; $\mu_1 = 1$ corresponds to the quasi-uniform mesh. Figure 9 shows the graded mesh with $h = 0.125$ and $\mu = \mu_3$.

The approximation errors and convergence rates are shown in Table 9 and Figure 10, where the notations are the same as in the previous subsection. We notice that $\beta_{\mu_1} < \beta_{\text{th}}$ for any discretization parameter h, where β_{th} is the theoretically predicted rate of convergence, and we know $\beta_{\text{th}} = \nu_0 + \frac{1}{2} \approx 0.792$ for the quasi-uniform meshes. This behaviour differs from the one for the reentrant edge case where $\beta_{\mu_1} > \beta_{\text{th}}$ for all h, see Tables 5 and 7. The convergence rates β_{μ_3} and β_{FSCM} given in Table 9 are very close to $\beta_{\text{th}} = 1$, namely the rate

h	e_{μ_1}	β_{μ_1}	e_{μ_2}	β_{μ_2}	e_{μ_3}	β_{μ_3}	e_{FSCM}	β_{FSCM}
0.25	3.982e-1	–	3.721e-1	–	3.350e-1	–	2.422e-1	–
0.125	2.608e-1	0.610	2.253e-1	0.724	1.654e-1	1.018	1.345e-1	0.849
0.0625	1.597e-1	0.708	1.276e-1	0.821	8.358e-2	0.984	7.079e-2	0.926
0.0312	9.521e-2	0.746	7.020e-2	0.862	4.243e-2	0.978	3.625e-2	0.966
0.0156	5.612e-2	0.763	3.806e-2	0.883	2.152e-2	0.979	1.832e-2	0.984
0.0078	3.279e-2	0.775	2.039e-2	0.900	1.089e-2	0.984	9.206e-3	0.993

Table 9: H^1-norms of approximation errors: e_{μ_1}, e_{μ_2}, e_{μ_3} and e_{FSCM}; and convergence rates β_{μ_1}, β_{μ_2}, β_{μ_3}, β_{FSCM} of the FFEM on both quasi-uniform meshes ($\mu_1 = 1$) and locally graded meshes ($\mu_2 \approx 0.808$, $\mu_3 \approx 0.634$) and of the FSCM.

predicted by theory, but the FSCM yields better approximation errors. As in the reentrant edge case, the mesh grading parameter $\mu_2 = 1.02\alpha \approx 0.808$ improves the convergence rate compared with quasi-uniform meshes, but the optimal rate is not achieved.
It should be mentioned that for the FSCM algorithm, the errors occurring due to the approximate evaluation of the Legendre function are negligible compared with the finite element discretization error [8, Remark 5.1].

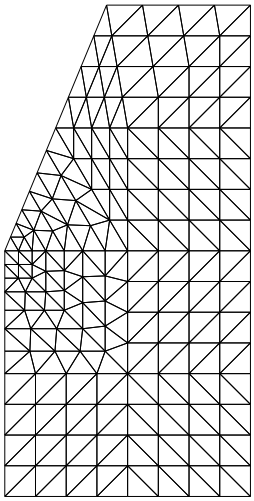

Figure 9: Graded mesh for $h = 0.125$ with $\mu \approx 0.634$

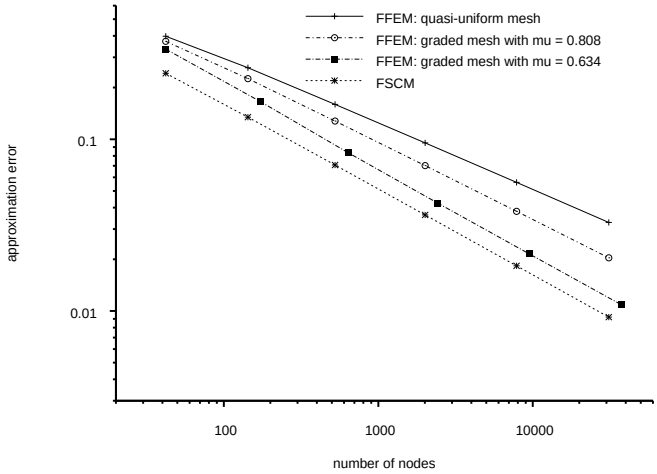

Figure 10: Representation of approximation errors for the example with the exact solution (16)

4 Study of the complexity of the algorithms

In this section, we shall analyse the computational complexities of the numerical algorithms which were tested in Sections 2 and 3. We start with the two methods FFEM and the FSCM, both of which involve finite element computations only in 2D. For the purpose, we

introduce the following notations:

K	-	number of Fourier modes used in an approximate solution;
$k_{\max}$	-	parameter used in the FSCM, given by $k_{\max} = [h^{-\frac{1}{2-\alpha}}]$, cf. Sections 2.2 and 3.1;
N_2	-	total number of nodes of the 2D finite element mesh;
ε	-	tolerance to stop the CG iteration in solving a linear system of equations;
k_0	-	characterizes the number of iterations for solving a linear system of equations. For each h there exists a number $k_{\mathrm{CG}}(h)$ such that the number of iterations to reach the tolerance ε in solving a linear system of equations by the preconditioned CG method is $\mathcal{O}(N_2^{\frac{3}{2}} \ln \varepsilon^{-1})$ for $k \le k_{\mathrm{CG}}(h)$ and $\mathcal{O}(N_2 \ln \varepsilon^{-1})$ for $k > k_{\mathrm{CG}}(h)$, with k being the Fourier index; we set $k_0 = k_{\mathrm{CG}}(h)$ in the FFEM complexity, and $k_0 = \min(k_{\mathrm{CG}}(h), k_{\max})$ in the FSCM complexity.
m	-	number of subintervals used for the algorithm of the Fast Fourier Transform;
q_1	-	number of quadrature points used for 1D integration;
q_2	-	number of quadrature points used for 2D integration.

First consider the FFEM. We know that for each k, the coefficient matrix $\mathbb{A}_{kh}$ involved in the resulting finite element system is of the form: $\mathbb{A}_{kh} = \mathbb{A}_h + k^2\mathbb{D}_h$ (cf. also [19, §6.1.1]), so the " stiffness " matrix $\mathbb{A}_h$ and the " mass " matrix $\mathbb{D}_h$ need to be generated only once. Moreover, it should be pointed out that for larger k, the part $k^2\mathbb{D}_h$ dominates in the coefficient matrix $\mathbb{A}_{kh}$. Consequently, the condition number of $\mathbb{A}_{kh}$ becomes more well-conditioned, thus the number of CG iterations for solving the linear system reduces.

Step of the algorithm	**Number of operations**
Generating the element stiffness matrices and the element mass matrices	$\mathcal{O}(q_2 N_2)$
Assembling the matrices $\mathbb{A}_h$ and $\mathbb{D}_h$	$\mathcal{O}(N_2)$
Computing the Fourier modes f^k of the right-hand side f in each quadrature point	$\mathcal{O}(q_2 N_2 m \log_2 m)$
Assembling the element right-hand sides for $k = 1, \ldots, K$	$\mathcal{O}(q_2 N_2 K)$
Solving K systems of linear equations using the preconditioned CG method	$\mathcal{O}(k_0 N_2^{\frac{3}{2}} \ln \varepsilon^{-1}) +$ $\mathcal{O}((K - k_0) N_2 \ln \varepsilon^{-1})$
Fourier synthesis of the solutions of the 2D problems	$\mathcal{O}(N_2 m \log_2 m)$

Table 10: Number of arithmetic operations needed for the FFEM in case of prismatic and axisymmetric domains

In Table 10, the number of operations is given for FFEM in both axisymmetric and prismatic domains, although it has been implemented only in axisymmetric domains (cf. Section 3). We know that the FFEM algorithm for prismatic domains is analogous to that for axisymmetric domains, and the FSCM algorithm contains all steps of the FFEM.

We see from Table 10 that the total number of operations for the FFEM may be

estimated by

$$\mathcal{O}(q_2 N_2 K \,+\, q_2 N_2 m \log_2 m \,+\, k_0 N_2^{\frac{3}{2}} \ln \varepsilon^{-1} + (K - k_0) N_2 \ln \varepsilon^{-1}). \tag{17}$$

When the FSCM is applied, we additionally have to take into account the number of operations which are needed to compute the dual and primal singular functions, the coefficients c_h^k and the regular parts $\tilde{u}_h^k$ for each $k = 0, \ldots, k_{\max}$. Let us mention that the computation of the dual and primal singular functions does not require any Fourier transform since the right-hand sides as well as the boundary functions of the corresponding 2D BVPs are explicitly known. For prismatic domains the dual and primal singular functions are the same for all k, therefore two systems of linear equations are to be generated and solved, and same for axisymmetric domains with a conical vertex. But for an axisymmetric domain with a reentrant edge, we have different dual (resp. primal) singular functions for $k = 0$, $|k| = 1$, and $|k| \geq 2$ (see (9), (10)), hence 6 systems of linear equations occur.

For computing the regular parts $\tilde{u}_h^k$, the matrices $\mathbb{A}_h$, $\mathbb{D}_h$, and the right-hand sides do not need to be generated again and can be taken from the algorithm of the FFEM. We have to compute only the bilinear form $a_k(\varphi_s^h, v)$ for the prismatic case (cf. Subsection 2.2) and for the axisymmetric case (with $\varphi_s^{0,e;h}$, $\varphi_s^{1;h}$, and $\varphi_s^{2;h}$ for a reentrant edge and $\varphi_s^{0,c;h}$ for a sharp vertex, cf. Subsections 3.1, 3.2). This leads to the complexity estimates in the following table.

Step of the algorithm	**Number of operations**
Generating the linear systems of equations for the dual and primal singular functions	$\mathcal{O}(q_2 N_2)$
Solving the systems of linear equations using the preconditioned CG method	$\mathcal{O}(N_2^{\frac{3}{2}} \ln \varepsilon^{-1})$
Computing the coefficients c_h^k for all $k = 1, \ldots, k_{\max}$	$\mathcal{O}(q_2 N_2 k_{\max})$
Computing the bilinear form $a_k(\varphi_s^h, v)$ for all $k = 1, \ldots, k_{\max}$	$\mathcal{O}(q_2 N_2 k_{\max})$
Solving $k_{\max}$ systems of linear equations using the preconditioned CG method (if $k_{\max} > k_0$)	$\mathcal{O}(k_0 N_2^{\frac{3}{2}} \ln \varepsilon^{-1})+$ $\mathcal{O}((k_{\max} - k_0) N_2 \ln \varepsilon^{-1})$
Solving the 2D problems: $u_h^k = \tilde{u}_h^k + c_h^k \varphi_s^h$, $k = 1, \ldots, k_{\max}$	$\mathcal{O}(k_{\max} N_2)$

Table 11: Number of arithmetic operations additionally needed for the FSCM in prismatic and axisymmetric domains

We see from Table 11 that the number of additional operations for the FSCM can be bounded by

$$\mathcal{O}(q_2 N_2 k_{\max} \,+\, k_0 N_2^{\frac{3}{2}} \ln \varepsilon^{-1} \,+\, (k_{\max} - k_0) N_2 \ln \varepsilon^{-1}). \tag{18}$$

In order to estimate the number of operations for those algorithms involving finite element computations in 3D for prismatic domains, i.e. the FEM with prismatic elements and the combined method discussed in Section 2.3, we add the following notations :

N_1 - number of nodes along the edge direction;
N_3 - total number of nodes of the 3D finite-element mesh;
q_3 - number of quadrature points used for 3D integration.

Noting that for the finite element meshes used in Section 2.1, we have the relations: $q_2 q_1 = q_3$, $N_2 N_1 = N_3$, and the regularity of the meshes implies $N_1 \approx h^{-1} \approx \sqrt{N_2}$. Moreover, for the parameter $k_{\max}$ used in the FSCM algorithm, we have $k_{\max} \approx h^{-\frac{1}{2-\alpha}} \approx N_2^{\frac{1}{2(2-\alpha)}}$.

When prismatic finite elements are used to solve the 3D problem, one needs to consider only the assembling of the stiffness matrix and the right-hand side, and the cost arising from the CG algorithm. These are reported in Table 12, from which we know the total number of operations for the prismatic finite element method can be estimated by

$$\mathcal{O}(q_2 N_2 q_1 N_1 + (N_1 N_2)^{\frac{4}{3}} \ln \varepsilon^{-1}). \tag{19}$$

Step of the algorithm	**Number of operations**
Generating the element stiffness matrix	$\mathcal{O}(q_2 N_2 q_1 N_1)$
Assembling the stiffness matrix	$\mathcal{O}(N_2 N_1)$
Assembling the right-hand side	$\mathcal{O}(N_1 q_1 N_2 q_2)$
Solving a linear system using the CG method	$\mathcal{O}((N_1 N_2)^{\frac{4}{3}} \ln \varepsilon^{-1})$

Table 12: Number of arithmetic operations needed for the 3D FEM in prismatic domains.

The discretization of the singular part involved in the FSCM requires to compute the Fourier modes f^k of the data f and u^k of the solution u approximately. The number of Fourier modes used to get the approximation of the singular part of u by the FSCM algorithm is h-dependent as outlined in Section 2.3, and only $k_{\max}$ modes are needed to obtain the approximation of the singular part.

The number of operations required for this method is summarized in Table 13, where $\mathbb{A}_h$ and $\mathbb{D}_h$ are respectively the stiffness and the mass matrix of the 2D Fourier modes problems. The numbers of operations for 3D computations are the same as in Table 12.

In summary, the combined method of prismatic finite elements with FSCM leads to a total number of operations of the following order :

$$\begin{aligned}\mathcal{O}((N_1 N_2)^{\frac{4}{3}} \ln \varepsilon^{-1} + N_1 q_1 N_2 q_2 + k_0 N_2^{\frac{3}{2}} \ln \varepsilon^{-1} + (k_{\max} - k_0) N_2 \ln \varepsilon^{-1} \\ + q_2 N_2 k_{\max} + q_2 N_2 m \log_2 m),\end{aligned} \tag{20}$$

Step of the algorithm	**Number of operations**
Generating the 2D stiffness matrices related to the dual and primal singular functions	$\mathcal{O}(q_2 N_2)$
Solving the systems of linear equations using the preconditioned CG method	$\mathcal{O}(N_2^{\frac{3}{2}} \ln \varepsilon^{-1})$
Assembling the matrices $\mathbb{A}_h$ and $\mathbb{D}_h$	$\mathcal{O}(N_2)$
Computing the Fourier modes f^k of the right-hand side f in each quadrature point	$\mathcal{O}(q_2 N_2 m \log_2 m)$
Assembling the right-hand sides for $k = 1, \ldots, k_{\max}$	$\mathcal{O}(q_2 N_2 k_{\max})$
Solving $k_{\max}$ linear systems of equations using the preconditioned CG method (if $k_{\max} > k_0$)	$\mathcal{O}(k_0 N_2^{\frac{3}{2}} \ln \varepsilon^{-1})+$ $\mathcal{O}((k_{\max} - k_0) N_2 \ln \varepsilon^{-1})$
Computing the coefficients c_h^k for all $k = 1, \ldots, k_{\max}$	$\mathcal{O}(q_2 N_2 k_{\max})$
Fourier synthesis of the $c_h^k \varphi_s^h$ for $k = 1, \ldots, k_{\max}$	$\mathcal{O}(N_2 m \log_2 m)$

Table 13: Number of arithmetic operations needed for the FSCM discretization of the singular part of the solution in prismatic domains.

which shows that the most expensive part of the combined method lies in the 3D solution of the linear system with a complexity $\mathcal{O}(N_2^2 \ln \varepsilon^{-1})$ and the FFT algorithm with a complexity $\mathcal{O}(N_2^{\frac{3}{2}} q_2 \ln(N_2))$.

Remark 4.1 *It should be mentioned that the number m of the subintervals for the FFT implementation depends on the number K of Fourier modes used, and we should have $m \geq 2(K+1)$. As far as the FSCM is concerned, the number K of Fourier modes used was chosen to ensure $K \geq h^{-1}$ for both prismatic and axisymmetric domains, see Sections 2.2 and 3.1. In contrast, the combined 3D FEM with FSCM requires only to compute $k_{max} \approx h^{-\frac{1}{2-\alpha}}$ Fourier modes ($\alpha = 2/3$) for prismatic domains, see Table 13. Consequently, the parameter m for this method can be chosen to be smaller than that of the FSCM.*

To compare the complexities, assume that $k_0 = k_{\max}$ for the FSCM (worst complexity). In one hand, if one recalls that $K \geq k_{\max}$, the complexities of the FSCM (18) and of the FFEM (17) are equivalent. On the other hand, when expressed in terms of the numbers of 2D degrees of freedom, the complexity of the FSCM is $O(N_2^{2-\eta} \ln \varepsilon^{-1})$, with $\eta = \frac{1-\alpha}{2(2-\alpha)} > 0$ that is slightly better than that of the 3D methods.

5 Conclusion

The numerical tests demonstrate that the FSCM always leads to optimal H^1-convergence in both the prismatic and the axisymmetric domains. It is especially interesting to observe that FSCM yields optimal convergence rates even when the right hand sides do not satisfy

the additional boundary condition on $\partial\omega\times\{0,1\}$ in the prismatic case or have less regularity with respect to z such as $f \in H_0^{1-s}(]0,1[;L^2(\omega))$. In the case of axisymmetric domains with a reentrant edge, the convergence in terms of the discretization parameter N outperforms the expected theoretical rate if u is more regular than $H^2(]0,2\pi[)$ with respect to θ, or equivalently f is more regular than $L_2(]0,2\pi[)$ with respect to θ (see Section 3.1). Moreover, the numerical experiments confirm that the convergence rates in terms of N are almost identical for all investigated methods. Concerning the complexities (see Section 4), the number of operations needed for the FSCM or the FFEM is slightly better than that of the 3D methods. It should be pointed out that, even if a large number N of Fourier modes are used, the number $k_{\max}$ of additional problems to be solved for the FSCM is not very large in comparison with N (cf. Tables 2 and 5).

References

[1] T. Apel. *Anisotropic finite elements: local estimates and applications.* B. G. Teubner, Advances in Numerical Mathematics, 1999.

[2] C. Bernardi, M. Dauge and Y. Maday. *Spectral methods for axisymmetric domains.* Series in Applied Mathematics, Gauthiers-Villars, Paris and North Holland, Amsterdam, 1999.

[3] S.C. Brenner, S. Nicaise and L.-Y. Sung. Multigrid methods for the computation of edge tensor product singular functions. *In preparation.*

[4] H. Blum. Numerical treatment of corner and crack singularities. In *Finite Element and Boundary Element Techniques from Mathematical and Engineering Point of View (eds. E. Stein, W. Wendland)*, 172-212, Wien-New York, 1988. CISM No. 301, Springer-Verlag.

[5] C. Canuto, M.Y. Hussaini, A. Quarteroni and T. A. Zang. *Spectral Methods in Fluid Dynamics.* Springer-Verlag, New York, 1988.

[6] P.G. Ciarlet. *Basic error estimates for elliptic problems.* in *Handbook of Numerical Analysis, Volume II (eds. P. G. Ciarlet, J.–L. Lions)*, 17-351, 1991. North Holland.

[7] P. Ciarlet, Jr, B. Jung, S. Kaddouri, S. Labrunie and J. Zou. The Fourier Singular Complement Method for the Poisson problem. Part I: prismatic domains. Accepted for publication in *Numerische Mathematik* (2005).

[8] P. Ciarlet, Jr, B. Jung, S. Kaddouri, S. Labrunie and J. Zou. The Fourier Singular Complement Method for the Poisson problem. Part II: axisymmetric domains. Accepted for publication in *Numerische Mathematik* (2005).

[9] P. Ciarlet, Jr and J. He. The Singular Complement Method for 2d problems. *C.R.Acad. Sci. Paris, Ser. I 336*:353-358, 2003.

[10] P. Grisvard. Singular solutions of elliptic boundary value problems in polyhedra. *Portugaliae Mathematica*, Vol. 41, Fasc. 1-4-1982.

[11] P. Grisvard. *Singularities in boundary value problems.* RMA 22, Masson, Paris, 1992.

[12] B. Heinrich. The Fourier-finite-element method for elliptic problems in axisymmetric domains. *Numerical treatment of coupled systems. Proceedings of the 11th GAMM-Seminar, Kiel, Germany, January 20-22, 1995* (W. Hackbusch et al., Eds.), pp. 59-72, Wiesbaden: Vieweg, 1995.

[13] B. Heinrich. The Fourier-finite-element-method for Poisson's equation in axisymmetric domains with edges. *SIAM J. Numer. Anal.*, 33:1885-1911, 1996.

[14] M. Jung and T. Steidten. Das Multigrid-Programmsystem FEMGP zur Lösung elliptischer und parabolischer Differentialgleichungen (Programmdokumentation). Technische Universität Chemnitz. (in preparation)

[15] J.L. Lions and E. Magenes. *Problèmes aux limites non homogènes et applications.* Volume 1, Dunod, Paris, 1968.

[16] B. Mercier and G. Raugel. Résolution d'un problème aux limites dans un ouvert axisymétrique par éléments finis en r, z et séries de Fourier en θ. *R.A.I.R.O. Analyse numérique*, 16(4):405-461, 1982.

[17] L.A. Oganesjan and L.A. Ruchovec. *Variacionno-raznostnye metody rešenija ellipličeskich uravnenij.* Izd. Akad. Nauk Armjanskoj SSR, Erevan, 1979.

[18] G. Raugel. Résolution numérique par une méthode d'éléments finis du problème de Dirichlet pour le laplacien dans un polygone. *C.R.Acad.Sci.Paris, Sér. A*, 286(18):A791-A794, 1978.

[19] B. Weber. *Die Fourier-Finite-Elemente-Methode für elliptische Interfaceprobleme in axialsymmetrischen Gebieten.* PhD thesis, Technische Universität Chemnitz-Zwickau, 1994.

[20] E. Stephan and J.R. Whiteman. Singularities of the Laplacian at corners and edges of three dimensional domains and their treatment with finite element methods. *Math. Meth. Appl. Sci., 10*: 339-350, 1988.

Other titles in the SFB393 series:

03-01 E. Creusé, G. Kunert, S. Nicaise. A posteriory error estimation for the Stokes problem: Anisotropic and isotropic discretizations. January 2003.

03-02 S. I. Solov'ëv. Existence of the guided modes of an optical fiber. January 2003.

03-03 S. Beuchler. Wavelet preconditioners for the p-version of the FEM. February 2003.

03-04 S. Beuchler. Fast solvers for degenerated problems. February 2003.

03-05 A. Meyer. Stable calculation of the Jacobians for curved triangles. February 2003.

03-06 S. I. Solov'ëv. Eigenvibrations of a plate with elastically attached load. February 2003.

03-07 H. Harbrecht, R. Schneider. Wavelet based fast solution of boundary integral equations. February 2003.

03-08 S. I. Solov'ëv. Preconditioned iterative methods for monotone nonlinear eigenvalue problems. March 2003.

03-09 Th. Apel, N. Düvelmeyer. Transformation of hexahedral finite element meshes into tetrahedral meshes according to quality criteria. May 2003.

03-10 H. Harbrecht, R. Schneider. Biorthogonal wavelet bases for the boundary element method. April 2003.

03-11 T. Zhanlav. Some choices of moments of refinable function and applications. June 2003.

03-12 S. Beuchler. A Dirichlet-Dirichlet DD-pre-conditioner for p-FEM. June 2003.

03-13 Th. Apel, C. Pester. Clément-type interpolation on spherical domains - interpolation error estimates and application to a posteriori error estimation. July 2003.

03-14 S. Beuchler. Multi-level solver for degenerated problems with applications to p-version of the fem. *(Dissertation)* July 2003.

03-15 Th. Apel, S. Nicaise. The inf-sup condition for the Bernardi-Fortin-Raugel element on anisotropic meshes. September 2003.

03-16 G. Kunert, Z. Mghazli, S. Nicaise. A posteriori error estimation for a finite volume discretization on anisotropic meshes. September 2003.

03-17 B. Heinrich, K. Pönitz. Nitsche type mortaring for singularly perturbed reaction-diffusion problems. October 2003.

03-18 S. I. Solov'ëv. Vibrations of plates with masses. November 2003.

03-19 S. I. Solov'ëv. Preconditioned iterative methods for a class of nonlinear eigenvalue problems. November 2003.

03-20 M. Randrianarivony, G. Brunnett, R. Schneider. Tessellation and parametrization of trimmed surfaces. December 2003.

04-01 A. Meyer, F. Rabold, M. Scherzer. Efficient Finite Element Simulation of Crack Propagation. February 2004.

04-02 S. Grosman. The robustness of the hierarchical a posteriori error estimator for reaction-diffusion equation on anisotropic meshes. March 2004.

04-03 A. Bucher, A. Meyer, U.-J. Görke, R. Kreißig. Entwicklung von adaptiven Algorithmen für nichtlineare FEM. April 2004.

04-04 A. Meyer, R. Unger. Projection methods for contact problems in elasticity. April 2004.

04-05 T. Eibner, J. M. Melenk. A local error analysis of the boundary concentrated FEM. May 2004.

04-06 H. Harbrecht, U. Kähler, R. Schneider. Wavelet Galerkin BEM on unstructured meshes. May 2004.

04-07 M. Randrianarivony, G. Brunnett. Necessary and sufficient conditions for the regularity of a planar Coons map. May 2004.

04-08 P. Benner, E. S. Quintana-Ortí, G. Quintana-Ortí. Solving Linear Matrix Equations via Rational Iterative Schemes. October 2004.

04-09 C. Pester. Hamiltonian eigenvalue symmetry for quadratic operator eigenvalue problems. October 2004.

04-10 T. Eibner, J. M. Melenk. An adaptive strategy for hp-FEM based on testing for analyticity. November 2004.

04-11 B. Heinrich, B. Jung. The Fourier-finite-element method with Nitsche-mortaring. November 2004.

04-12 A. Meyer, C. Pester. The Laplace and the linear elasticity problems near polyhedral corners and associated eigenvalue problems. December 2004.

04-13 M. Jung, T. D. Todorov. On the Convergence Factor in Multilevel Methods for Solving 3D Elasticity Problems. December 2004.

05-01 C. Pester. A residual a posteriori error estimator for the eigenvalue problem for the Laplace-Beltrami operator. January 2005.

05-02 J. Badía, P. Benner, R. Mayo, E. Quintana-Ortí, G. Quintana-Ortí, J. Saak. Parallel Order Reduction via Balanced Truncation for Optimal Cooling of Steel Profiles. February 2005.

05-03 C. Pester. CoCoS – Computation of Corner Singularities. April 2005.

05-04 A. Meyer, P. Nestler. Mindlin-Reissner-Platte: Einige Elemente, Fehlerschätzer und Ergebnisse. April 2005.

05-05 P. Benner, J. Saak. Linear-Quadratic Regulator Design for Optimal Cooling of Steel Profiles. April 2005.

05-06 A. Meyer. A New Efficient Preconditioner for Crack Growth Problems. April 2005.

05-07 A. Meyer, P. Steinhorst. Überlegungen zur Parameterwahl im Bramble-Pasciak-CG fr gemischte FEM. April 2005.

05-08 T. Eibner, J. M. Melenk. Fast algorithms for setting up the stiffness matrix in hp-FEM: a comparison. June 2005.

05-09 A. Meyer, P. Nestler. Mindlin-Reissner-Platte: Vergleich der Fehlerindikatoren in Bezug auf die Netzsteuerung Teil I. June 2005.

05-10 A. Meyer, P. Nestler. Mindlin-Reissner-Platte: Vergleich der Fehlerindikatoren in Bezug auf die Netzsteuerung Teil II. July 2005.

05-11 A. Meyer, R. Unger. Subspace-cg-techniques for clinch-problems. September 2005.

The complete list of current and former preprints is available via
`http://www.tu-chemnitz.de/sfb393/preprints.html`.